

1 **Title: *Limosilactobacillus reuteri*-derived tripeptide SKL exerts**
2 **antibacterial activity against systemic and wound infections via**
3 **dual membrane-killing and anti-virulence mechanisms**

4
5 **Authors:** Qi Lu ^{a, b}, Di Wang ^a, Haojie Jing ^a, Haijian Wang ^{a, b}, Na Li ^a, Baikui Wang ^a,
6 ^c, Longhai Yu ^a, Yifei Feng ^{a, b}, Liyuan Mo ^a, Kun Zhou ^a, Min Yue ^{a, c}, Yan Li ^{a, b*}

7
8 **Affiliations:**

9 a MOA Key Laboratory of Animal Virology & Zhejiang Provincial Engineering Research
10 Center of Animal Biological Products, Zhejiang University College of Animal Sciences,
11 Hangzhou, Zhejiang 310058, China

12 b Hainan Institute of Zhejiang University, Sanya, Hainan 572025, China

13 c Key Laboratory of Systems Health Science of Zhejiang Province, School of Life
14 Science, Hangzhou Institute for Advanced Study, University of Chinese Academy of
15 Sciences, Hangzhou, Zhejiang 310024, China

16

17 *Corresponding author: Yan Li, yanli3@zju.edu.cn

18

19

20 **ABSTRACT**

21 The escalating crisis of antimicrobial resistance (AMR) necessitates innovative
22 antimicrobial strategies beyond conventional antibiotics. Although the beneficial
23 effects of probiotics are well recognized, the specific molecular effectors responsible
24 for their systemic protective functions remain largely unexplored. Here, we screened
25 the piglet gut microbiota and identified *Limosilactobacillus reuteri* P190 as a strain with
26 potent, broad-spectrum activity against diverse bacterial pathogens and robust
27 protection against lethal systemic *Salmonella* infection *in vivo*. Mechanistic
28 investigations revealed that this protective effect is attributed to a novel tripeptide, Ser-
29 Lys-Leu (SKL). SKL exerts a unique dual mode of action: it rapidly disrupts bacterial
30 cell membranes at inhibitory concentrations, while simultaneously attenuating
31 virulence by targeting the QseC quorum-sensing system even at sub-inhibitory
32 concentrations. Notably, through tandem-repeat engineering, we developed a highly
33 potent variant, (SKL)₄, which dramatically enhances direct antimicrobial efficacy while
34 retaining low hemolysis and cytotoxicity. Both SKL and (SKL)₄ protect mice from lethal
35 systemic *Salmonella* challenges independent of host immunity, demonstrating their
36 direct, autonomous therapeutic power. Furthermore, topical applications of these
37 peptides successfully cleared methicillin-resistant *Staphylococcus aureus* wound
38 infections and accelerated healing, with efficacy comparable to that of mupirocin.
39 Collectively, our findings identify SKL as a promising probiotic-derived lead
40 antimicrobial peptide with dual membrane-disrupting and anti-virulence capabilities,
41 offering a compelling strategy to combat multidrug-resistant pathogens.

42

43 **KEYWORDS:** Gut microbiome; *Limosilactobacillus reuteri*; tripeptide SKL;
44 antimicrobial peptide (AMP); QseC

45 Introduction

46 Antimicrobial resistance (AMR) remains one of the most urgent threats to global
47 health. According to the most recent comprehensive global estimate, bacterial AMR
48 was estimated to have directly caused 1.14 million deaths and to have been
49 associated with an additional 4.71 million deaths; by 2050, these numbers are
50 projected to increase to 1.91 million and 8.22 million, respectively.¹ The growing
51 burden is driven by clinically important resistant pathogens that continue to undermine
52 the efficacy of existing antibiotics and expose the limitations of current antibacterial
53 development pipelines. These challenges underscore the urgent need for new
54 antibacterial agents and innovative therapeutic strategies to solve antibiotic
55 resistance.^{1, 2}

56 Antimicrobial peptides (AMPs) have emerged as promising next-generation anti-
57 infective agents.³ Unlike many conventional antibiotics which typically act on specific
58 enzymatic or biosynthetic targets, AMPs often exert rapid and broad-spectrum activity
59 by disrupting bacterial membranes.^{4, 5} Their cationic and amphipathic properties
60 promote preferential interactions with bacterial envelopes, resulting in membrane
61 destabilization, depolarization, pore formation, and leakage of intracellular contents.⁵
62 ⁶ Although AMPs are generally considered less susceptible to classical resistance,
63 bacterial envelope remodeling and other adaptive responses can still diminish AMP
64 activity *in vivo*.^{4, 7} Therefore, a pressing need remains to discover and characterize
65 novel AMPs to combat the growing threat of antimicrobial resistance.

66 The host-associated microbiome represents an evolutionarily selected reservoir of
67 bioactive molecules shaped by ecological competition, microbial coexistence, and
68 host adaptation.^{8, 9} Machine-learning approaches have recently enabled the prediction
69 and identification of active AMPs from both the human gut microbiome and global
70 microbial metagenomes.^{10, 11} Among gut commensals, probiotic lactic acid bacteria
71 (LAB) are recognized as producers of diverse antimicrobial metabolites, and large-
72 scale genomic mining coupled with machine learning has further expanded the
73 repertoire of LAB-derived AMPs.¹² However, due to their cationic and amphipathic

74 nature, AMPs are often associated with adverse effects such as hemolysis or
75 nephrotoxicity, with stronger bactericidal activity frequently correlating with a greater
76 propensity for off-target toxicity.¹³ Most high-throughput screening platforms prioritize
77 direct bactericidal activity and *in vitro* potency, while the *in vivo* effects, including
78 suppression of virulence, biofilm formation, and antibody-assisted bacterial clearance,
79 as well as adverse effects, are often undetermined.¹⁴⁻¹⁶

80 Here, we identified a probiotic-derived tripeptide, SKL, with broad antibacterial
81 activity isolated from piglet gut microbes. Tandem-repeat engineering optimized it into
82 (SKL)₄, showing enhanced charge, structure, and potency with host safety. Both SKL
83 and (SKL)₄ exert rapid bactericidal effects via membrane disruption; SKL also inhibits
84 virulence by downregulating QseC, thereby impairing biofilm formation. In murine
85 models of both systemic and localized infection, SKL and (SKL)₄ significantly reduced
86 bacterial burdens and improved disease outcomes without overt toxicity. Thus, SKL is
87 a microbiome-derived lead AMP that integrates direct membrane-targeted killing with
88 targeted anti-virulence activity, highlighting the value of ecological discovery and
89 rational engineering for antimicrobial development.

90

91 **Materials and Methods**

92 **Bacterial strains and culture conditions**

93 A complete list of bacterial strains and culture conditions is provided in
94 Supplementary Methods. In brief, *Salmonella* Typhimurium SL1344 and the other
95 bacterial strains used in this study were maintained under species-appropriate growth
96 conditions.

97

98 **Antimicrobial peptide characterization and in vitro assays**

99 The identification of the secreted tripeptide SKL, synthesis of tandem-repeat
100 derivatives, and all in vitro antimicrobial assays, including MIC/MBC determination,
101 time-kill kinetics, hemolysis, mammalian cell viability, biofilm inhibition, resistance
102 passage, and membrane-damage assays, are described in Supplementary Methods.

103

104 **Mouse experiments**

105 All animal procedures were approved by the Institutional Animal Care and Use
106 Committee of Zhejiang University and were performed under Animal Biosafety Level
107 2 (ABSL2) containment. Mice were housed under specific-pathogen-free conditions
108 with free access to sterile water and autoclaved chow.

109 For the systemic *Salmonella* infection model, C57BL/6 mice received P190, P190
110 cell-free supernatant, or protease-digested supernatant before and after oral
111 challenge with *S. Typhimurium* SL1344, whereas SKL and (SKL)₄ were evaluated in
112 separate prophylactic and therapeutic regimens via the indicated routes of
113 administration. Mice were monitored for body weight, survival, and bacterial burden in
114 target organs at the indicated time points. To determine whether peptide activity
115 required host immunity, a cyclophosphamide-induced neutropenic mouse model was
116 used. To assess whether the in vivo effect of SKL was mediated by microbiota
117 remodeling, a fecal microbiota transplantation experiment was performed. To verify
118 QseC-dependent virulence suppression in vivo, a competitive infection assay using a

119 1:1 mixture of wild-type and $\Delta qseC$ *S. Typhimurium* was conducted. For localized
120 infection, BALB/c mice were used in a full-thickness MRSA wound infection model and
121 treated topically with SKL ointment, (SKL)₄ ointment, mupirocin, or vehicle control.
122 Detailed protocols for each animal model are provided in Supplementary Methods.

123

124 **Generation of *qseC* knockout and complemented strains**

125 The *qseC* deletion mutant ($\Delta qseC$) was constructed using the pCas/pTarget
126 CRISPR-Cas9-assisted λ Red recombination system, and the complemented strain
127 (C- $\Delta qseC$) was generated by introducing a pACYC184-based plasmid carrying the
128 *qseC* gene with its native promoter into the $\Delta qseC$ mutant. Detailed procedures are
129 provided in Supplementary Methods.

130

131 **qRT-PCR and Western blot analysis**

132 Quantitative real-time PCR, bacterial protein extraction, Western blot analysis, and
133 primer information are described in Supplementary Methods.

134

135 **Statistical analysis**

136 Statistical analysis is described in Supplementary Methods.

137

138 **Result**

139 **Gut-derived *Limosilactobacillus reuteri* P190 confers protection against** 140 **systemic *Salmonella* infection in mice**

141 The healthy livestock gut harbors a rich community of symbiotic microbes with
142 documented probiotic potential.¹⁷ Among these, gut-derived LAB are particularly well-
143 adapted to the host environment and have been shown to counteract bacterial
144 infections through the production of broad-spectrum antimicrobial metabolites.¹⁸ From
145 the intestinal contents of one-month-old healthy piglets, we isolated 750 bacterial
146 strains, of which 325 were identified as LAB by matrix-assisted laser
147 desorption/ionization time-of-flight mass spectrometry (MALDI-TOF MS), including 26
148 strains of *Limosilactobacillus reuteri* (**Figure 1a**). Using an agar well-diffusion assay,
149 we screened all 325 LAB isolates for antibacterial activity (**Supplemental Table S1**).
150 All 26 *L. reuteri* strains exhibited activity against a panel of clinically relevant
151 pathogens (*Enterococcus faecium*, *Staphylococcus aureus*, *Klebsiella pneumoniae*,
152 *Acinetobacter baumannii*, *Pseudomonas aeruginosa*, and *Salmonella* Typhimurium)
153 with a general preference for Gram-negative over Gram-positive bacteria. Among
154 these strains, strain P190 displayed the strongest inhibitory effect, whereas strain
155 P126 showed the weakest (**Figure 1b**). Notably, P190 was the most potent inhibitor
156 of *Salmonella* Typhimurium of the set.

157 Encouraged by the robust *in vitro* activity of P190 against *S. Typhimurium*, we next
158 assessed its protective efficacy *in vivo* using a mouse model of systemic *S.*
159 *Typhimurium* infection. C57BL/6 mice orally received P190 or PBS daily for 7 days
160 prior to *S. Typhimurium* infection, with treatments continuing thereafter (**Figure 1c**).
161 Whereas all PBS-treated control mice succumbed to infection by day 7, showing rapid
162 and severe weight loss, P190-treated mice exhibited significantly prolonged survival,
163 with 30% (3/10) still alive at 20 days post-infection (dpi) (**Figures 1d, 1e**). At 3 dpi, *S.*
164 *Typhimurium* colony-forming units (CFUs) recovered from liver, spleen, and cecal
165 contents of P190-treated mice were 4-126 times fewer than from PBS-treated mice.
166 Furthermore, only 2 of 6 blood samples from P190-treated mice had detectable

167 bacteria, and those counts approached the detection limit (**Figure 1f**).

168 Histological examination of liver and spleen at 3 dpi corroborated these findings.
169 Compared with mock-infected control mice, PBS-treated mice displayed severe organ
170 damage: livers showed disrupted architecture and widespread inflammatory foci, while
171 spleens exhibited extensive structural disorganization, sparse white-pulp lymphocytes,
172 heavy neutrophil infiltration of the red pulp, and diffuse lymphocyte necrosis. In
173 contrast, P190-treated mice developed only mild inflammatory changes in both liver
174 and spleen, with no obvious tissue necrosis or architecture disruption (**Figures 1g,**
175 **1h**). Collectively, these results demonstrate that *L. reuteri* P190 confers potent
176 protection against systemic *S. Typhimurium* SL1344 infection in mice.

177

178 **The secreted tripeptide SKL is the principal antimicrobial effector of *L.*** 179 ***reuteri* P190**

180 To pinpoint the active antibacterial component of *L. reuteri* P190, we first separated
181 the whole culture into a bacteria-free supernatant and a bacteria pellet and tested each
182 fraction against *S. Typhimurium* SL1344 using an agar diffusion assay. Strong
183 antimicrobial activity was observed in both the whole culture and the supernatant, but
184 not in the pellet (**Figure 2a**), indicating that the primary antibacterial effector is a
185 secreted metabolite rather than bacterial cells or their structural components.

186 We next characterized the biochemical nature of this effector. Untreated
187 supernatant completely inhibited bacterial growth within 2-4 hours. This activity was
188 markedly reduced by treatment with trypsin but unaffected by pepsin (**Figures 2b, 2c**),
189 suggesting that the active factor is a peptide or protein sensitive to trypsin yet resistant
190 to gastric pepsin. In a mouse model of *S. Typhimurium* infection, untreated P190
191 supernatant significantly improved survival and lowered bacterial loads, whereas
192 trypsin pretreatment eliminated these effects (**Figures 2d-2g**), confirming the
193 peptide-dependent protection *in vivo*.

194 To identify the specific antibacterial peptide, we fractionated the P190 supernatant.
195 Antimicrobial activity was observed exclusively in the <3 kDa fraction (**Figure S1a**)

196 and was protease-sensitive (**Figures S1b and S1c**), indicating that the activity was
197 attributable to a small peptide. Untargeted metabolomics was then performed on P190
198 supernatant, with P126 as a control. Principal component analysis (PCA) revealed
199 clear separation of the two metabolomes (**Figure 2h**), indicating distinct metabolite
200 profiles. Of 716 differentially expressed metabolites, 278 were upregulated and 438
201 were downregulated in P190 (**Supplemental Table S2**). Amino acids and their
202 derivatives (58 metabolites) and organic acids and derivatives (42 metabolites) were
203 the most abundant categories (**Figure 2i**), consistent with the observation that NaOH
204 neutralization reduced antibacterial activity (**Figure S1d, S1e**). Among upregulated
205 amino-acid-related differentially expressed metabolites (\log_2 fold change > 1), only two
206 peptides longer than two residues were found: the tripeptides Ala-Pro-Lys (APK) and
207 Ser-Lys-Leu (SKL) (**Figure 2j**). Structural and sequence analysis of SKL predicted a
208 cleavage site for trypsin but no canonical pepsin cleavage motif (**Figure 2k, 2l**).
209 Notably, SKL showed broad-spectrum activity against a panel of clinically relevant
210 Gram-negative and Gram-positive pathogens (**Figure S2a**), with a minimum inhibitory
211 concentration (MIC) of 128 $\mu\text{g}/\text{mL}$ against *S. Typhimurium* SL1344 (**Figure 2m**).
212 Trypsin treatment raised the MIC to 256 $\mu\text{g}/\text{mL}$, whereas pepsin had no effect (**Figure**
213 **2m**). APK, in contrast, exhibited substantially weaker activity, with MIC values ranging
214 from 2.5 to 10 mg/mL against the tested pathogens (**Figures S2b, S2c**), and its MIC
215 remained unchanged upon trypsin or pepsin treatment (**Figure S2d**). Together, these
216 data identify tripeptide SKL as the principal antimicrobial peptide secreted by *L. reuteri*
217 P190.

218 **Tandem-repeat optimization of SKL enhances antimicrobial activity**

219 The tripeptide SKL showed only modest activity against *S. Typhimurium* (MIC = 128
220 $\mu\text{g}/\text{mL}$), considerably weaker than polymyxin B, which typically exhibits MIC values of
221 0.25–2 $\mu\text{g}/\text{mL}$ against most susceptible Gram-negative pathogens.¹⁹ To improve its
222 potency, we turned to rational design. SKL carries a positive charge and hydrophobic
223 residues, which are characteristic of antimicrobial peptides and facilitate binding to
224 negatively charged bacterial membranes. Moreover, its C-terminal leucine is known to

225 stabilize α -helical structure in amphipathic AMPs.²⁰ We reasoned that the short length
226 of the tripeptide limited its charge density, amphipathicity, and helical stability.
227 Accordingly, we synthesized tandem repeats of the SKL motif in 3, 4, 5, 6, or 9 copies
228 (designated (SKL)₃ - (SKL)₉) via solid-phase synthesis to augment net cationic charge
229 and hydrophobic moment while promoting α -helix formation via the repeating leucine
230 residues. AlphaFold secondary-structure prediction confirmed stable α -helices in all
231 constructs (**Figure 3a**), supporting our design rationale.

232 We next evaluated the antimicrobial activity of the SKL repeats against 17 bacterial
233 strains, including Gram-negative and Gram-positive pathogens, as well as probiotic
234 lactobacilli. (SKL)₄ and (SKL)₅ reduced the MIC against *S. Typhimurium* SL1344 to 8
235 $\mu\text{g/mL}$, equivalent to a 16-fold improvement over native SKL (**Figure 3b**). However,
236 further extension to 6 or 9 copies did not enhance antimicrobial potency; instead, the
237 MIC increased for most strains (**Figure 3b**), suggesting the optimal peptide length is
238 critical for maintaining antimicrobial efficacy. Notably, all repeats displayed broad-
239 spectrum activity but were more potent against Gram-negative (MIC 8-64 $\mu\text{g/mL}$) than
240 against Gram-positive bacteria (MIC 32-128 $\mu\text{g/mL}$). Inhibitory activity against *L.*
241 *reuteri* P190 and other lactobacilli was minimal (MIC > 256 $\mu\text{g/mL}$). Biocompatibility
242 testing revealed low hemolysis (<2%) and high mammalian cell viability (>95%) for
243 SKL, (SKL)₃, and (SKL)₄, whereas (SKL)₅ and longer repeats caused increased
244 hemolysis and reduced viability (**Figure 3c**). Time–kill assays against *S. Typhimurium*
245 SL1344 showed that (SKL)₄ achieved complete bacterial clearance at 1 \times MBC within
246 1.5 hours, compared to 9 hours for SKL (**Figure 3d**), indicating that (SKL)₄ achieved
247 markedly faster bactericidal kinetics. Based on these results, we selected (SKL)₄ for
248 further characterization.

249 Lastly, we tested the likelihood of resistance emergence by passaging *S.*
250 *Typhimurium* and methicillin-resistant *S. aureus* (MRSA) to 20 passages in
251 subinhibitory concentrations ($\frac{1}{2}\times\text{MIC}$) of SKL or (SKL)₄, with polymyxin B and
252 vancomycin as controls. No MIC increase was observed for either SKL or (SKL)₄ after
253 20 passages, whereas MICs for polymyxin B and vancomycin rose 32-fold and 8-fold,
254 respectively (**Figures 3e, 3f**). Thus, tandem-repeat optimization enhances bactericidal

255 potency without driving rapid resistance, consistent with the known low resistance
256 propensity of membrane-active AMPs.^{21 22}

257

258 **SKL and (SKL)₄ specifically disrupt bacterial cell membranes**

259 The cationic and amphipathic nature of SKL and (SKL)₄ suggests a membrane-
260 disruptive mechanism, similar to that of antimicrobial peptides. To visualize this, we
261 examined treated bacterial cells using scanning electron microscopy (SEM). Exposure
262 to SKL or (SKL)₄ at 1×MIC for 1 hour caused severe morphological alterations,
263 including cell shrivelling, surface irregularities, and the formation of membrane
264 ruptures and holes. This structural damage was more pronounced with (SKL)₄
265 treatment than with SKL (**Figure 4a**). Likewise, MRSA cells displayed distinct
266 membrane distortions and leakage of intracellular contents following treatment with
267 SKL or (SKL)₄ (**Figure 4a**).

268 Membrane permeabilization was further quantified via fluorescence assays. SKL
269 and (SKL)₄ gradually increased the N-phenyl-1-naphthylamine (NPN) fluorescence
270 intensity, and they elicited a 20-fold increase in NPN fluorescence intensity relative to
271 the PBS vehicle following a 6-hour treatment, demonstrating a substantial increase in
272 the outer-membrane (OM) permeability of *S. Typhimurium* post SKL- and (SKL)₄
273 treatment (**Figure 4b**). Moreover, a significant rise in inner-membrane (IM)
274 permeability was observed as early as 60 minutes for SKL and 40 minutes for (SKL)₄,
275 with the permeability peaking at 120 minutes for SKL and at 80 minutes for (SKL)₄. In
276 both assays, (SKL)₄ induced greater membrane permeability than SKL (**Figure 4c**).
277 Consistent with these findings, SKL and (SKL)₄ triggered rapid leakage of intracellular
278 nucleic acids and proteins, with (SKL)₄ mediating a faster efflux rate (**Figures 4d, 4e**).
279 Notably, the membrane-disruptive potency of (SKL)₄ was comparable to that of
280 polymyxin B (**Figures S3a, S3b**).

281 Furthermore, SKL and (SKL)₄ treatment significantly altered the biophysical
282 properties of the bacterial membrane, characterized by increased fluidity and
283 decreased hydrophobicity compared to vehicle controls (**Figures 4f, 4g**). Reduced

284 membrane hydrophobicity compromises structural stability, while elevated fluidity
285 disrupts membrane order; these synergistic effects undermine membrane integrity²³
286 and facilitate the observed cellular leakage. Together, these data confirm that SKL and
287 (SKL)₄ kill bacteria by disrupting membrane integrity, aligning with the established
288 mechanism of membrane-active antimicrobial peptides.

289

290 **SKL and (SKL)₄ protect mice from systemic *Salmonella* infection** 291 **independent of host immunity**

292 Having established the *in vitro* potency of SKL and (SKL)₄, we next assessed their
293 therapeutic potential *in vivo* using murine models of systemic *S. Typhimurium* infection.
294 Dose optimization in immunocompetent C57BL/6 mice revealed that a single daily
295 intraperitoneal (i.p.) injection of 25 mg/kg SKL for 3 days reduced bacteria loads in the
296 liver, spleen, and blood to below the limit of detection; cecal *S. Typhimurium* CFUs
297 were 5000 times lower than those in vehicle-treated controls (**Figures S4a, S4b**).
298 While oral gavage required a higher dose (50 mg/kg) to achieve comparable efficacy
299 (**Figure S4c**), i.p. 25 mg/kg (SKL)₄ was sufficient to clear systemic infection (**Figure**
300 **S4d**). At this optimized dose, both peptides rescued mice from lethal infection,
301 mitigating weight loss and improving 20-day survival to 60% with SKL and 80% with
302 (SKL)₄, whereas all vehicle-treated control mice succumbed within one week (**Figures**
303 **S4e, S4f**). Histological examination of liver and spleen at 3 dpi revealed that compared
304 to mock mice, vehicle-treated mice displayed extensive hepatic and splenic
305 destruction with rampant inflammation, whereas SKL- and (SKL)₄-treated mice
306 retained largely normal organ architecture, including intact hepatocyte nuclei, well-
307 formed hepatic cords, and spleens with preserved follicles and clear red/white pulp
308 boundaries, with only minimal focal inflammation (**Figures S4g, S4h**). Importantly,
309 serum alanine aminotransferase (ALT) and blood urea nitrogen (BUN) levels remained
310 unchanged relative to vehicle-treated controls, indicating this protection occurred
311 without hepatotoxicity or nephrotoxicity (**Figures S5a, S5b**). We also tested
312 prophylactic administration: pre - infection treatment with either peptide produced

313 similar outcomes, reducing bacterial loads in the liver, spleen, and cecal contents to
314 approximately 1.6%–5% of vehicle control levels and extending survival by 3–10 days
315 **(Figures S6a-c)**, confirming that SKL and (SKL)₄ confer robust therapeutic and
316 prophylactic protection against systemic *Salmonella* infection.

317 To determine whether this protection arises from direct antimicrobial action rather
318 than host-mediated effects, we evaluated peptide efficacy in a neutropenic mouse
319 model. Flow cytometry analysis confirmed that cyclophosphamide pretreatment
320 significantly depleted peripheral blood CD8⁺ T cells, B cells, and neutrophils compared
321 to untreated controls **(Figures S7a, S7b)**. Cyclophosphamide-pretreated mice were
322 infected with *S. Typhimurium* and administered 25 mg/kg SKL, (SKL)₄, or vehicle via
323 i.p. injection at 2 h, 24 h, and 48 h post-infection **(Figure 5a)**. While all PBS-treated
324 mice died by day 5, peptide-treated mice showed attenuated weight loss and
325 significantly extended survival, with 30% of mice surviving to the end of the
326 observation period **(Figures 5b, 5c)**. At 2 dpi, SKL- and (SKL)₄-treated mice harbored
327 126-3162 times fewer *S. Typhimurium* CFUs in the liver, spleen, and cecum; blood
328 bacterial loads fell to near the detection limit, whereas vehicle-treated mice exhibited
329 severe bacteremia **(Figure 5d)**. These data confirmed that SKL and (SKL)₄ protect
330 mice from systemic bacterial infection independent of host immunity.

331 Finally, to exclude indirect protection mediated by microbiota remodeling, we
332 performed fecal microbiota transplantation. Recipient mice colonized with microbiota
333 from SKL-treated donors showed no survival advantage or reduction in tissue bacterial
334 loads following *S. Typhimurium* infection compared to recipients of vehicle-treated
335 microbiota **(Figures S8a-c)**. Thus, the *in vivo* efficacy of SKL and (SKL)₄ is not
336 mediated by shifts in microbial community but rather reflects direct antibacterial activity.
337 This result excludes major microbiota-mediated effects and confirms that SKL's *in vivo*
338 efficacy is principally due to its direct antimicrobial action. Intriguingly, while (SKL)₄
339 exhibits superior membrane disruption and antimicrobial activity *in vitro*, SKL and
340 (SKL)₄ confer equivalent protection *in vivo*, suggesting that SKL may regulate specific
341 signaling pathways that compensate for its lower direct lytic activity.

342

343 **SKL suppresses virulence by targeting the QseC quorum-sensing system**

344 Bacterial biofilm formation drives antibiotic resistance and persistent infection.²⁴ We
345 therefore tested whether SKL and (SKL)₄ inhibit *S. Typhimurium* biofilm formation. SKL
346 significantly inhibited *Salmonella* biofilm formation even at subinhibitory concentration
347 ($\frac{1}{4}\times$ MIC). Although (SKL)₄ achieved biofilm eradication at $1\times$ MIC comparable to
348 polymyxin B at $4\times$ MIC, it failed to reduce biofilm formation at $\frac{1}{4}\times$ MIC (**Figure 6a**). This
349 $\frac{1}{4}\times$ MIC concentration is well below the MIC of SKL and insufficient to exert direct
350 bactericidal effects, suggesting that SKL possesses unique subinhibitory mechanisms
351 that (SKL)₄ lacks, possibly linked to the regulation of biofilm formation.

352 Given that biofilm formation is regulated by amino-acid-sensing signaling,²⁵ we
353 screened four well-known bacterial signaling systems that sense amino acid or peptide
354 signals to regulate biofilm formation and virulence: QseB/QseC,²⁶ PhoP/PhoQ,^{27, 28}
355 Lrp,²⁹ and CpxA/CpxR.³⁰ Quantifying the transcription of their central regulator (*qseC*,
356 *phoP*, *lrp*, *cpxA*) revealed that only *qseC* was significantly downregulated by SKL
357 (**Figure 6b**). At $1\times$ MIC, SKL reduced *qseC* mRNA levels by $\sim 84.5\%$ in *S. Typhimurium*
358 SL1344, whereas *phoP*, *lrp*, and *cpxA* expression remained unchanged (**Figure 6b**).
359 Importantly, the tetramer (SKL)₄, which lacks biofilm-inhibitory activity at subinhibitory
360 concentrations, did not affect *qseC* expression, establishing a strong correlation
361 between QseC modulation and biofilm formation phenotype. Dose-response analysis
362 showed that SKL at $\frac{1}{4}\times$ MIC, $\frac{1}{2}\times$ MIC and $1\times$ MIC progressively lowered *qseC* transcript
363 levels (**Figure 6c**). At $\frac{1}{4}\times$ MIC of SKL, *qseC* mRNA level fell by $\sim 62.2\%$, and biofilm
364 formation was similarly reduced (**Figure 6a**). This parallel dose-dependency
365 suggested a causal relationship between QseC suppression and the anti-biofilm
366 activity of SKL. Western Blot confirmed that SKL markedly reduced QseC protein
367 abundance of *S. Typhimurium* (**Figure 6d**). To confirm the specificity of SKL on QseC,
368 we generated a strain with *qseC* knockout ($\Delta qseC$) and a complemented strain (C-
369 $\Delta qseC$) in the background of *S. Typhimurium* SL1344. QseC was absent in the $\Delta qseC$
370 regardless of SKL treatment, whereas C- $\Delta qseC$ recapitulated the response of the wild-
371 type (WT) strain, showing 31.4% reduction in QseC protein levels after SKL treatment.
372 These data identify QseC as the target through which SKL disrupts biofilm formation

373 and virulence.

374 QseC is a histidine kinase in the QseB/QseC two-component system that
375 phosphorylates the response regulator QseB to regulate key virulence traits,²⁶
376 including genes from *Salmonella* pathogenicity island 1 (SPI-1) for epithelial cell
377 invasion, genes from *Salmonella* pathogenicity island 2 (SPI-2) for intracellular
378 replication, and flagellar genes for bacterial motility and colonization (**Figure 6e**). We
379 examined six representative targets: *hilD* and *sipA* (SPI-1), *ssaV* and *sifA* (SPI-2), and
380 *flhDC* and *fliC* (flagellar regulation). Treatment with SKL significantly reduced the
381 expression of all six genes by 50.0%-77% in the WT strain. In contrast, in the $\Delta qseC$
382 mutant, SKL had no effect on these gene expressions, and complementation with
383 *qseC* fully restored SKL sensitivity (**Figure 6f–k**). Furthermore, the expression of these
384 six genes was dose-dependently suppressed by SKL, with progressive reductions
385 observed from $\frac{1}{4}\times$ MIC to $1\times$ MIC (**Figure S9a–f**). These results demonstrate that SKL
386 acts through QseC to broadly suppress virulence gene expression, functionally
387 attenuating the pathogen.

388 To test whether this anti-QseC mechanism contributes to antimicrobial activity *in*
389 *vivo* and to further separate anti-virulence effect from direct bactericidal activity, we
390 established a subinhibitory dose of SKL that has no direct bactericidal activity. At
391 5 mg/kg, SKL did not significantly reduce bacterial loads in the liver, spleen, or cecal
392 contents compared to vehicle controls (**Figure S4b**), indicating minimal direct killing.
393 Nevertheless, this dose of SKL improved mouse survival by 40%, whereas (SKL)₄
394 exhibited no protective efficacy (**Figure S10**). To further confirm that SKL's *in vivo*
395 protection relies on QseC suppression, we used the same subinhibitory SKL dose and
396 performed a competitive infection experiment. Mice were co-infected with a 1:1 mixture
397 of WT and $\Delta qseC$ *Salmonella* strains, followed by SKL or PBS treatment. We then
398 determined the competitive index (CI) (CI= $\Delta qseC$ CFU / WT CFU) in the liver, spleen,
399 ileum, cecal contents, and feces (**Figure 6I**). In PBS-treated controls, CI was below 1
400 in the liver (~ 0.37), spleen (~ 0.40), and ileum (~ 0.43), confirming that the $\Delta qseC$
401 strain is less fit in these organs due to its virulence defect. In the cecal contents and
402 feces, CIs were near or above 1 (~ 1.10), indicating active shedding of the $\Delta qseC$

403 strain. Strikingly, SKL treatment raised the CI to near unity across all tissues (liver
404 ~0.85, spleen ~0.89, ileum ~0.90, cecal contents ~1.02, feces ~1.05) (**Figure 6m**).
405 This shift demonstrates that SKL attenuates the WT strain's competitive advantage by
406 inhibiting its QseC system, effectively phenocopying the $\Delta qseC$ mutant *in vivo*.
407 Therefore, beyond any direct bactericidal activity, SKL provides a second layer of
408 defense by disabling the QseC quorum-sensing circuit during infection.

409

410 **Topical SKL and (SKL)₄ clear MRSA wound infections in mice**

411 Given the growing clinical challenge due to multidrug-resistant pathogens such as
412 methicillin-resistant *Staphylococcus aureus* (MRSA),³¹ we next tested whether SKL
413 and (SKL)₄ could treat localized wound infections by MRSA. We formulated SKL and
414 (SKL)₄ into topical ointments and assessed their efficacy in a mouse model of MRSA-
415 infected full-thickness skin wound (**Figure 7a**). Mice received either SKL ointment,
416 (SKL)₄ ointment, mupirocin (standard-of-care antibiotic),³² or a vehicle control
417 ointment. Wound closure was monitored on 3, 5, 7, 9, and 11 dpi. Both SKL and (SKL)₄
418 markedly accelerated wound healing compared to PBS vehicle, as shown by serial
419 photographs (**Figure 7b**) and quantified by heatmap visualization of wound area
420 dynamics (**Figure 7c**). Healing rates were significantly higher in both SKL and (SKL)₄
421 treatment groups at all time points (**Figure 7d**). By day 11, SKL treatment achieved
422 98.69% wound closure, which was no less than 98.17% observed with mupirocin,
423 indicating potent therapeutic equivalence. Consistent with the improved healing, SKL
424 and (SKL)₄ substantially reduced bacterial load in wound tissue. Both treatments with
425 SKL and (SKL)₄ reduced MRSA CFU to 1.58% of vehicle control levels (**Figure 7e**),
426 comparable to mupirocin, highlighting their potential as alternative topical antimicrobial
427 agents.

428

429 Discussion

430 The growing global burden of antimicrobial resistance (AMR) necessitates
431 innovative strategies beyond conventional antibiotics.¹ The gut microbiome, shaped
432 by long-term ecological selection, represents a natural reservoir of bioactive molecules
433 whose peptide components often exhibit favorable host compatibility and stability *in*
434 *vivo*.³³ In this study, we characterized a microbiome-derived tripeptide, SKL, secreted
435 by a *Limosilactobacillus reuteri* P190 from the healthy piglet gut, which exhibits a
436 distinct, concentration-dependent dual mechanism of action. At bactericidal
437 concentration, SKL acts as a rapid membrane-disruptive agent; at sub-inhibitory
438 regimes, it functions as an anti-virulence modulator by targeting the histidine kinase
439 QseC. This bifunctional architecture of SKL introduces a programmable therapeutic
440 framework: high-dose regimens can be deployed for acute, high-burden pathogen
441 clearance, whereas low-dose interventions offer a precision-medicine approach to
442 reduce pathogenesis while preserving the ecological integrity of the commensal
443 microbiota.

444 Across a panel of 26 distinct *L. reuteri* isolates, we observed preferential activity
445 against Gram-negative to Gram-positive pathogens. Our metabolomic and
446 biochemical analyses revealed a high abundance of organic acids within the P190
447 supernatant, with neutralization assays confirming that acidification provides a critical
448 physiological backdrop for inhibition. Concurrently with the well-established secretion
449 of reuterin by this species,³⁴ our data support a model wherein *L. reuteri* P190
450 coordinates a multi-tiered antimicrobial offense: co-secreted organic acids lower the
451 microenvironmental pH and destabilize target homeostasis, thereby acting as auxiliary
452 agents that facilitate the primary, peptide-mediated membrane disruption. This
453 cooperative secretome architecture highlights the clinical necessity of transitioning
454 from single-metabolite isolation to ecological, multi-factorial screening paradigms
455 during probiotic and postbiotic development.

456 A key advantage of SKL is its low propensity to induce resistance. Through 20 serial
457 passages, neither the native peptide SKL nor its tandem repeats (SKL)₄ elicited any

458 detectable increase in MIC, contrasting sharply with the rapid resistance kinetics
459 observed for the clinical counter-selections polymyxin B and vancomycin. This
460 durability stems from fundamentally different mechanistic constraints. Pathogen
461 resistance to polymyxin B typically involves discrete genetic adaptations. Specifically,
462 PhoPQ/PmrAB-mediated lipid A remodeling or mcr-driven phosphoethanolamine
463 transfer that neutralizes outer-membrane surface charge.³⁵⁻³⁷ Similarly, vancomycin
464 resistance relies on target site alterations or pronounced cell-wall thickening to
465 sequester the drug.^{38, 39} In contrast, the antibacterial activity of SKL is governed by a
466 collective, biophysical interplay of its three residues: Lysine (K) drives electrostatic
467 attraction to anionic outer bacterial membranes;^{40, 41} leucine (L) mediates hydrophobic
468 insertion to destabilize the bilayer core;^{42, 43} and serine (S) fine-tunes overall
469 amphiphilicity, promoting stable intramembrane aggregation and enhancing disruption
470 of Gram-negative bacterial membranes.⁴⁴ By anchoring its bactericidal efficacy to
471 global physical properties of the bacterial lipid bilayer rather than a single mutable
472 protein receptor, SKL imposes a high evolutionary hurdle; pathogen escape would
473 require macro-scale physiological remodeling of membrane composition, a trajectory
474 typically accompanied by prohibitive biological fitness.⁴⁵

475 The multi-valent engineering further highlights that the optimal peptide length is
476 critical in peptide design. While tandem concatenation is a recognized tool to amplify
477 peptide potency by increasing effective valency/avidity and promoting productive
478 membrane engagement,^{46, 47} excessive lengthening frequently introduces over-
479 hydrophobicity, rendering candidates susceptible to self-aggregation⁴⁸ and reducing
480 free bioavailability⁴⁹. Our finding that extending the SKL motif to 6 or 9 severely
481 compromised antimicrobial performance identifies (SKL)₄ as a highly optimized
482 thermodynamic sweet spot. This tetramer successfully balances charge density,
483 hydrophobic moment, and structural helicity, offering an engineering blueprint for
484 calibrating the therapeutic index of short, ultra-small peptide scaffolds.

485 The QseC inhibitor, LED209, selectively blocks signal binding to QseC, preventing
486 its autophosphorylation and thereby dampening QseC-dependent virulence gene
487 expression without impacting growth dynamics. LED209 provided robust protection in

488 *Salmonella* models, although it did not influence *S. typhimurium* growth *in vitro*.⁵⁰
489 However, SKL integrates QseC-linked virulence suppression with direct membrane
490 disruption and bactericidal activity. At subinhibitory concentrations, SKL
491 downregulates *qseC* transcription and inhibits biofilm formation; while at bactericidal
492 concentrations, it disrupts membranes and achieves complete killing. This dual-layer
493 constraint effectively prevents QseC-dependent pathogen motility and invasion, which
494 is conserved in many Gram-negative enteric pathogens,²⁶ while the membrane-lytic
495 component handles strains lacking the target, such as MRSA. Consequently, the
496 clinical spectrum of SKL is defined by a unique intersection of membrane vulnerability
497 and signaling circuitry, making it uniquely suited for complex clinical indications where
498 high bacterial burdens and aggressive virulence expression simultaneously drive host
499 tissue damage.

500 Lastly, the striking disconnect observed between *in vitro* potency and *in vivo* efficacy
501 reveals a nuanced pharmacokinetic reality. Despite (SKL)₄ demonstrating a 16-fold
502 superior *in vitro* MIC against *S. Typhimurium* relative to monomeric SKL, both
503 candidates yielded nearly indistinguishable survival benefits in systemic murine
504 infection models. This lack of linear translation strongly points to complex physiological
505 buffers, including differential proteolytic degradation, high serum-protein binding, or
506 distinct tissue clearance rates that restrict the free-drug exposure of the larger tetramer
507 at infected foci. Crucially, the sub-MIC anti-virulence activity unique to monomeric SKL
508 is a therapeutic synergy completely masked by standard *in vitro* MIC assays. This
509 positions SKL as a highly competitive clinical candidate. Their robust performance in
510 MRSA-infected wound models, even matching the clinical standard mupirocin,
511 highlights their potential as topical therapeutics for ischemic, hypoxic chronic wounds
512 such as diabetic foot ulcers, where conventional antibiotic options are rapidly being
513 exhausted.⁵¹ Nevertheless, further work is required to evaluate the therapeutic
514 potential of SKL and (SKL)₄ in these and additional clinically relevant models, as well
515 as to define their long-term safety, the evolution of resistance under host-relevant
516 conditions, and the molecular basis of the SKL-QseC interaction.

517

518 **Conclusions**

519 We demonstrate that *L. reuteri* P190, isolated from the piglet gut, exhibits strong
520 antimicrobial activity both *in vitro* and *in vivo*. We further identified the tripeptide SKL
521 as the primary effector molecule underpinning this antibacterial effect. Rational
522 engineering into the tetravalent derivative (SKL)₄ improved charge distribution,
523 conformational stability, and antibacterial potency while preserving host compatibility.
524 Both SKL and (SKL)₄ act rapidly by disrupting bacterial membranes and confer robust
525 protection against systemic and localized bacterial infections in murine models.
526 Notably, at sub-inhibitory concentrations, SKL additionally attenuates virulence via
527 suppression of QseC-dependent signaling, thereby impairing biofilm formation and
528 pathogenicity. Collectively, this study unveils SKL as a novel antimicrobial peptide
529 motif and underscores the value of ecological discovery and rational engineering for
530 antimicrobial development.

531

532 **Funding Statement**

533 This work was supported by Zhejiang Province “San Nong Jiu Fang” Science and
534 Technology Cooperation Program (2026SNJF040), the National Program on Key
535 Research Project of China (2019YFE0103900), and Hangzhou Chengxi Sci-tech
536 innovation Corridor Management Committee.

537

538 **Acknowledgments**

539 We thank Jiajia Wang and Yingying Huang from the Core Facilities, Zhejiang
540 University School of Medicine for their technical supports. We also thank Yulan Jin,
541 Xueqiu Chen, Weidong Zeng and Dandan Liu from the Experimental Teaching Center,
542 College of Animal Sciences, Zhejiang University for using the qPCR instrument
543 (LightCycler® 480 II, Roche).

544

545

546 **Declaration of Interest Statement**

547 The other authors have no conflict of interest to declare

548

549 **Data Availability Statement**

550 The metabolomics data generated in this study have been deposited on Figshare
551 (<https://doi.org/10.6084/m9.figshare.32791506>). All other data supporting the findings
552 of this study are available from the corresponding author upon reasonable request.

553

554 **Author contributions**

555 Y L, Q L, M Y and BK W provide experimental ideas and design the study. Q L, D
556 W, HJ J, HJ W, N L, LH Y, YF F, LY M and K Z conducted the experiments. Q L and
557 HJ W analyzed and interpreted the data. Q L and Y L drafted the manuscript. Y L
558 reviewed and edited the manuscript.

559

560 **References**

- 561 1. Collaborators GAR. Global burden of bacterial antimicrobial resistance 1990-2021: a systematic
562 analysis with forecasts to 2050. *Lancet (London, England)* 2024; 404:1199-226.
- 563 2. Sati H, Carrara E, Savoldi A, Hansen P, Garlasco J, Campagnaro E, et al. The WHO Bacterial
564 Priority Pathogens List 2024: a prioritisation study to guide research, development, and public health
565 strategies against antimicrobial resistance. *The Lancet Infectious diseases* 2025; 25:1033-43.
- 566 3. Oliveira Júnior NG, Souza CM, Buccini DF, Cardoso MH, Franco OL. Antimicrobial peptides:
567 structure, functions and translational applications. *Nature reviews Microbiology* 2025; 23:687-700.
- 568 4. Wang Y, Zhao L, Li Z, Xi Y, Pan Y, Zhao G, et al. A generative artificial intelligence approach for the
569 discovery of antimicrobial peptides against multidrug-resistant bacteria. *Nature microbiology* 2025;
570 10:2997-3012.
- 571 5. Chen EH, Wang CH, Liao YT, Chan FY, Kanaoka Y, Uchihashi T, et al. Visualizing the membrane
572 disruption action of antimicrobial peptides by cryo-electron tomography. *Nature communications* 2023;
573 14:5464.
- 574 6. Bhaumik KN, Spohn R, Dunai A, Daruka L, Olajos G, Zákány F, et al. Chemically diverse
575 antimicrobial peptides induce hyperpolarization of the E. coli membrane. *Communications biology* 2024;
576 7:1264.
- 577 7. Tajer L, Paillart JC, Dib H, Sabatier JM, Fajloun Z, Abi Khattar Z. Molecular Mechanisms of
578 Bacterial Resistance to Antimicrobial Peptides in the Modern Era: An Updated Review. *Microorganisms*
579 2024; 12:1259.
- 580 8. Wang Y, Shi YN, Xiang H, Shi YM. Exploring nature's battlefield: organismic interactions in the
581 discovery of bioactive natural products. *Natural product reports* 2024; 41:1630-51.
- 582 9. Hussain A, Patwekar U, Mongad DS, Shouche YS. Strategizing the human microbiome for small
583 molecules: Approaches and perspectives. *Drug discovery today* 2023; 28:103459.
- 584 10. Santos-Júnior CD, Torres MDT, Duan Y, Rodríguez Del Río Á, Schmidt TSB, Chong H, et al.
585 Discovery of antimicrobial peptides in the global microbiome with machine learning. *Cell* 2024;
586 187:3761-78.e16.
- 587 11. Ma Y, Guo Z, Xia B, Zhang Y, Liu X, Yu Y, et al. Identification of antimicrobial peptides from the
588 human gut microbiome using deep learning. *Nature biotechnology* 2022; 40:921-31.
- 589 12. Du R, Han F, Li Z, Yu J, Xu Y, Huang Y, et al. Uncovering encrypted antimicrobial peptides in health-
590 associated Lactobacillaceae by large-scale genomics and machine learning. *Microbiome* 2025; 13:151.
- 591 13. Javadi H, Lehnen AC, Hartlieb M. Bioinspired Cationic Antimicrobial Polymers. *Angewandte*
592 *Chemie (International ed in English)* 2025; 64:e202503738.
- 593 14. Castillo-Juárez I, Blancas-Luciano BE, García-Contreras R, Fernández-Présas AM. Antimicrobial
594 peptides properties beyond growth inhibition and bacterial killing. *PeerJ* 2022; 10:e12667.
- 595 15. Daher R, Pouget C, Lavigne JP, François P, Dunyach-Remy C. Anti-virulence peptides: a
596 compromising strategy to treat *Staphylococcus aureus* chronic wound infection. *Critical reviews in*
597 *microbiology* 2026; 52:414-32.
- 598 16. Hairsine B, Leire E, Rostam HM, Kristian SA, Rhodes E, Johnson A, et al. Harnessing endogenous
599 anti-glycan antibodies using a novel, bifunctional immunotherapy to treat gram-negative bacterial
600 infections. *Journal of immunology (Baltimore, Md : 1950)* 2025; 214:1617-29.
- 601 17. Gorzelanna Z, Mamrot A, Będkowska D, Bubak J, Miszczak M. Exploring the Potential of Novel
602 Animal-Origin Probiotics as Key Players in One Health: Opportunities and Challenges. *International*

- 603 journal of molecular sciences 2025; 26:5143.
- 604 18. Teng K, Huang F, Liu Y, Wang Y, Xia T, Yun F, et al. Food and gut originated bacteriocins involved
605 in gut microbe-host interactions. *Critical reviews in microbiology* 2023; 49:515-27.
- 606 19. Jones RN, Anderegg TR, Swenson JM. Quality control guidelines for testing gram-negative control
607 strains with polymyxin B and colistin (polymyxin E) by standardized methods. *Journal of clinical*
608 *microbiology* 2005; 43:925-7.
- 609 20. Brango-Vanegas J, Leite ML, Macedo MLR, Cardoso MH, Franco OL. Capping motifs in
610 antimicrobial peptides and their relevance for improved biological activities. *Frontiers in chemistry* 2024;
611 12:1382954.
- 612 21. Zhong C, Zhang F, Yao J, Zhu Y, Zhu N, Zhang J, et al. New Antimicrobial Peptides with Repeating
613 Unit against Multidrug-Resistant Bacteria. *ACS infectious diseases* 2021; 7:1619-37.
- 614 22. Zhong C, He Y, Zou J, Gao L, Wang J, Zhu J, et al. An antimicrobial peptide as a potential therapy
615 for bacterial pneumonia that alleviates antimicrobial resistance. *Nature communications* 2025;
616 16:10488.
- 617 23. Guha S, Ghimire J, Wu E, Wimley WC. Mechanistic Landscape of Membrane-Permeabilizing
618 Peptides. *Chemical reviews* 2019; 119:6040-85.
- 619 24. Domouchtsidou A, Ioannou P, Lianou A, Tsante KA, Tsakri D, Bonova E, et al. Biofilms in clinical
620 infection: pathophysiology, diagnosis, and the evolving therapeutic landscape. *Journal of clinical*
621 *microbiology* 2025; 64:e0104225.
- 622 25. Yan C, Li X, Zhang G, Bi J, Hao H, Hou H. The Regulatory Role of Quorum Sensing-Mediated
623 Amino Acid Metabolism in Biofilm Formation and Motility of *Hafnia alvei* H4. *Foods (Basel, Switzerland)*
624 2026; 15:281.
- 625 26. Zhu Y, Dou Q, Du L, Wang Y. QseB/QseC: a two-component system globally regulating bacterial
626 behaviors. *Trends in microbiology* 2023; 31:749-62.
- 627 27. Bader MW, Sanowar S, Daley ME, Schneider AR, Cho U, Xu W, et al. Recognition of antimicrobial
628 peptides by a bacterial sensor kinase. *Cell* 2005; 122:461-72.
- 629 28. Yang H, Jiang X, Nychas GE, Yang K, Dong P, Zhang Y, et al. Role of the PhoP/PhoQ Two-
630 Component Regulatory System in Biofilm Formation in Acid-Adapted *Salmonella typhimurium*. *Foods*
631 *(Basel, Switzerland)* 2025; 14:4344.
- 632 29. Schachterle JK, Sundin GW. The Leucine-Responsive Regulatory Protein Lrp Participates in
633 Virulence Regulation Downstream of Small RNA ArcZ in *Erwinia amylovora*. *mBio* 2019; 10:e00757-19.
- 634 30. Li D, Shi Q, He L, Luo J, Zhu H, Hua X, et al. Cpx-mediated amino acid sensing diversifies
635 gastrointestinal colonization of *Klebsiella pneumoniae*. *mLife* 2025; 4:181-92.
- 636 31. Parsons JB, Mourad A, Conlon BP, Kielian T, Fowler VG, Jr. Methicillin-resistant and susceptible
637 *Staphylococcus aureus*: tolerance, immune evasion and treatment. *Nature reviews Microbiology* 2026;
638 24:127-45.
- 639 32. Septimus EJ, Schweizer ML. Decolonization in Prevention of Health Care-Associated Infections.
640 *Clinical microbiology reviews* 2016; 29:201-22.
- 641 33. Torres MDT, Brooks EF, Cesaro A, Sberro H, Gill MO, Nicolaou C, et al. Mining human microbiomes
642 reveals an untapped source of peptide antibiotics. *Cell* 2024; 187:5453-67.e15.
- 643 34. Ortiz-Rivera Y, Sánchez-Vega R, Gutiérrez-Méndez N, León-Félix J, Acosta-Muñiz C, Sepulveda
644 DR. Production of reuterin in a fermented milk product by *Lactobacillus reuteri*: Inhibition of pathogens,
645 spoilage microorganisms, and lactic acid bacteria. *Journal of dairy science* 2017; 100:4258-68.
- 646 35. Huang J, Li C, Song J, Velkov T, Wang L, Zhu Y, et al. Regulating polymyxin resistance in Gram-

- 647 negative bacteria: roles of two-component systems PhoPQ and PmrAB. *Future microbiology* 2020;
648 15:445-59.
- 649 36. Liu YY, Wang Y, Walsh TR, Yi LX, Zhang R, Spencer J, et al. Emergence of plasmid-mediated
650 colistin resistance mechanism MCR-1 in animals and human beings in China: a microbiological and
651 molecular biological study. *The Lancet Infectious diseases* 2016; 16:161-8.
- 652 37. Gao R, Hu Y, Li Z, Sun J, Wang Q, Lin J, et al. Dissemination and Mechanism for the MCR-1
653 Colistin Resistance. *PLoS pathogens* 2016; 12:e1005957.
- 654 38. Reynolds PE, Courvalin P. Vancomycin resistance in enterococci due to synthesis of precursors
655 terminating in D-alanyl-D-serine. *Antimicrobial agents and chemotherapy* 2005; 49:21-5.
- 656 39. Rose WE, Knier RM, Hutson PR. Pharmacodynamic effect of clinical vancomycin exposures on
657 cell wall thickness in heterogeneous vancomycin-intermediate *Staphylococcus aureus*. *The Journal of*
658 *antimicrobial chemotherapy* 2010; 65:2149-54.
- 659 40. Kumar P, Kizhakkedathu JN, Straus SK. Antimicrobial Peptides: Diversity, Mechanism of Action
660 and Strategies to Improve the Activity and Biocompatibility In Vivo. *Biomolecules* 2018; 8:4.
- 661 41. Wang J, Zeng F, Chen X, Wang T, Wang L, Zhou M, et al. Engineering of antimicrobial peptide
662 Brevinin-1pl: arginine, lysine, and histidine substitutions enhance antimicrobial-anticancer efficacy with
663 reduced cytotoxicity. *Frontiers in chemistry* 2025; 13:1579097.
- 664 42. Lobka M, Siekierska I, Chyży P, Burmistrz M, Macyszyn J, Grzela R, et al. Design, synthesis and
665 evaluation of lysine- and leucine-rich hydrocarbon-stapled peptides as antibacterial agents. *European*
666 *journal of medicinal chemistry* 2025; 290:117445.
- 667 43. Chen Y, Guarnieri MT, Vasil AI, Vasil ML, Mant CT, Hodges RS. Role of peptide hydrophobicity in
668 the mechanism of action of alpha-helical antimicrobial peptides. *Antimicrobial agents and chemotherapy*
669 2007; 51:1398-406.
- 670 44. Stephens A, Ge T, Ding K, Hollowell P, Clifton L, Hall S, et al. Selective Serine Substitutions of
671 Antimicrobial Peptides Reveal Different Mechanistic Actions Toward Gram-Negative Bacteria. *ACS*
672 *applied materials & interfaces* 2026; 18:10860-73.
- 673 45. Spohn R, Daruka L, Lázár V, Martins A, Vidovics F, Grézal G, et al. Integrated evolutionary analysis
674 reveals antimicrobial peptides with limited resistance. *Nature communications* 2019; 10:4538.
- 675 46. Liu SP, Zhou L, Lakshminarayanan R, Beuerman RW. Multivalent Antimicrobial Peptides as
676 Therapeutics: Design Principles and Structural Diversities. *International journal of peptide research and*
677 *therapeutics* 2010; 16:199-213.
- 678 47. Pratap Verma D, Ansari MM, Verma NK, Saroj J, Akhtar S, Pant G, et al. Tandem Repeat of a Short
679 Human Chemerin-Derived Peptide and Its Nontoxic d-Lysine-Containing Enantiomer Display Broad-
680 Spectrum Antimicrobial and Antitubercular Activities. *Journal of medicinal chemistry* 2021; 64:15349-66.
- 681 48. Thapa S, Gahlawat A, Schneebeli ST, Li J. Interplay of Hydrophobicity, Charge, and Sequence
682 Length in Oligopeptide Coassembly. *The Journal of Physical Chemistry B* 2025; 129:4383-91.
- 683 49. Acquah C, Di Stefano E, Udenigwe CC. Role of hydrophobicity in food peptide functionality and
684 bioactivity. *Journal of Food Bioactives* 2018; 4:88-98.
- 685 50. Rasko DA, Moreira CG, Li de R, Reading NC, Ritchie JM, Waldor MK, et al. Targeting QseC
686 signaling and virulence for antibiotic development. *Science (New York, NY)* 2008; 321:1078-80.
- 687 51. Tarigan MB, Saragih RM, Tarigan KA, Ginting F. Antimicrobial resistance and empirical antibiotic
688 use in diabetic foot infections: A retrospective study from Indonesia. *Narra J* 2025; 5:e2895.
- 689

690 **FIGURE LEGENDS**

691 **Figure 1. Gut-derived *Limosilactobacillus reuteri* P190 exhibits broad-spectrum** 692 **antibacterial activity and confers protection against systemic *Salmonella*** 693 ***Typhimurium* SL1344 infection in C57BL/6 mice.**

694 (a) Schematic of the sequential isolation and screening workflow from piglet
695 intestinal contents, showing the number and proportion of isolates at each step and
696 the ultimate identification of *L. reuteri* P190.

697 (b) Heatmap depicting the antimicrobial activity of 26 isolated *L. reuteri* strains
698 against a panel of clinically relevant pathogens. Inhibition zone diameters (mm) are
699 represented by a color gradient.

700 (c) Schematic of experimental timeline for the murine model of systemic *S.*
701 *Typhimurium* SL1344 infection.

702 (d, e) Body weight changes (d) and survival rates (e) of mice following *S.*
703 *Typhimurium* SL1344 infection (n = 10 per group).

704 (f) Bacterial loads (CFU) in the liver, spleen, cecal contents, and blood at 3 days
705 post-infection (dpi) (n = 6 per group). The dashed line indicates the limit of detection
706 (LOD).

707 (g, h) Histological examination of H&E-stained liver (g) and spleen (h) sections.
708 Mock group (uninfected, untreated) served as the healthy control. PBS-STM and
709 P190-STM groups were infected with *S. Typhimurium* SL1344 and received sterile
710 PBS or *L. reuteri* P190, respectively.

711 Data are shown as the mean \pm SD. Statistical significance for body weight changes
712 and bacteria loads was determined using two-way ANOVA, whereas survival curves
713 were analyzed using the log-rank (Mantel-Cox) test. * $p < 0.05$; ** $p < 0.01$; *** $p <$
714 0.001 ; ns, not significant.

715

716 **Figure 2. Identification of the secreted tripeptide SKL as the key antimicrobial** 717 **effector of *Limosilactobacillus reuteri* P190.**

718 (a) Antimicrobial activity of *L. reuteri* P190 whole culture (P190), cell-free

719 supernatant (P190 sup), and washed cell pellet (P190 pel) against *S. Typhimurium*
720 SL1344, assessed by agar well diffusion assay. The dashed line indicates the
721 threshold for detectable activity.

722 (b) Growth inhibition of *S. Typhimurium* SL1344 by MRS medium, untreated P190
723 cell-free supernatant (P190 sup), and P190 cell-free supernatant digested with pepsin
724 (P190 sup-pepsin) or trypsin (P190 sup-trypsin), monitored by OD₆₀₀ over 24 hours.

725 (c) Inhibition zone diameters of untreated P190 cell-free supernatant (Untreated)
726 and P190 cell-free supernatant digested with pepsin or trypsin against *S. Typhimurium*
727 SL1344, determined by agar well diffusion assay.

728 (d) Schematic of experimental timeline for the murine model of systemic *S.*
729 *Typhimurium* SL1344 infection.

730 (e, f) Body weight changes (e) and survival rates (f) of mice following *S.*
731 *Typhimurium* SL1344 infection (n = 10 per group).

732 (g) Bacterial loads (CFU) in the liver, spleen, cecal contents, and blood at 3 dpi (n
733 = 6 per group). The dashed line indicates the limit of detection (LOD).

734 (h) Principal component analysis (PCA) score plot of untargeted metabolomics data
735 from *L. reuteri* P190 and P126 cell-free supernatants. Ellipses represent the 95%
736 confidence intervals (n = 6 per group).

737 (i) Abundance ranking of differently expressed metabolites (DEM) identified
738 between P190 and P126 supernatants.

739 (j) Volcano plot of DEMs, highlighting metabolites significantly upregulated in P190
740 (log₂-fold change > 1, *p* < 0.05).

741 (k) Chemical structure of the tripeptide SKL (Ser-Lys-Leu) from PubChem.

742 (l) *In silico* prediction of trypsin and pepsin cleavage sites within the SKL sequence.

743 (m) Minimum inhibitory concentrations (MIC) of SKL against *S. Typhimurium*
744 SL1344, determined with or without prior digestion by pepsin or trypsin.

745 Data are shown as the mean ± SD. Statistical significance of body weight changes
746 and growth curves was assessed using one-way ANOVA or two-way ANOVA; survival
747 curves were compared using the log-rank (Mantel-Cox) test. * *p* < 0.05; ** *p* < 0.01;
748 *** *p* < 0.001; ns, not significant.

749

750 **Figure 3. Tandem-repeat optimization of SKL enhances antimicrobial activity**
751 **and establishes (SKL)₄ as the lead candidate.**

752 (a) AlphaFold-predicted secondary structures of SKL tandem-repeat peptides
753 (SKL)₃ through (SKL)₉.

754 (b) Bubble plot depicting the minimum inhibitory concentrations (MIC, µg/mL) of
755 SKL and its tandem-repeat peptides against a panel of bacterial strains indicated in
756 the figure. MIC values are encoded by both color intensity and bubble size, as defined
757 in the scale.

758 (c) Hemolytic activity and viability of RAW264.7 cells following treatment with SKL
759 and its tandem-repeat peptides.

760 (d) Time-kill kinetics of SKL and (SKL)₄ against *S. Typhimurium* SL1344 at 1×MIC
761 and 1× minimum bactericidal concentration (MBC).

762 (e, f) Development of resistance in *S. Typhimurium* SL1344(e) and in methicillin-
763 resistant *S. aureus* (MRSA) (f) under ½ x MIC concentrations of SKL, (SKL)₄,
764 polymyxin B, or vancomycin.

765 Data are shown as the mean ± SD. Statistical significance was assessed using one-
766 way ANOVA. * $p < 0.05$; ** $p < 0.01$; *** $p < 0.001$; ns, not significant.

767

768 **Figure 4. SKL and (SKL)₄ exert bactericidal activity through disrupting**
769 **membrane integrity.**

770 (a) Scanning electron microscopy (SEM) micrographs of *Salmonella* Typhimurium
771 SL1344 and methicillin-resistant *Staphylococcus aureus* (MRSA) cells treated with
772 SKL or (SKL)₄ at 1×MIC for 1 h. PBS-treated cells served as the vehicle control.

773 (b) Outer membrane permeability of *S. Typhimurium* SL1344 following treatment
774 with PBS vehicle, SKL, or (SKL)₄, measured via NPN fluorescence uptake assay.

775 (c) Inner membrane permeability of *S. Typhimurium* SL1344 treated with PBS
776 vehicle, SKL, or (SKL)₄, indicated by the hydrolysis of ONPG and monitored by OD₄₂₀.

777 (d, e) Leakage of cellular contents from *S. Typhimurium* SL1344 after treatment
778 with SKL or (SKL)₄ at 1×MIC for the indicated durations, determined by absorbance at

779 OD₂₆₀ for nucleic acid (d) and OD₂₈₀ for protein (e). PBS-treated cells were served as
780 vehicle control.

781 (f) Membrane fluidity of *S. Typhimurium* SL1344 treated with PBS vehicle, SKL, or
782 (SKL)₄, assessed by DPH fluorescence polarization assay.

783 (g) Membrane hydrophobicity of *S. Typhimurium* SL1344 treated with PBS vehicle,
784 SKL, or (SKL)₄, assessed by hexadecane partitioning assay.

785 Data are shown as the mean ± SD. Statistical significance was assessed by one-
786 way ANOVA. * $p < 0.05$; ** $p < 0.01$; *** $p < 0.001$; ns, not significant.

787

788 **Figure 5. SKL and (SKL)₄ confer protection against systemic *Salmonella***
789 **infection in immunocompromised neutropenic mice.**

790 (a) Schematic of experimental timeline for the cyclophosphamide-induced
791 neutropenic murine model of systemic *S. Typhimurium* SL1344 infection.

792 (b, c) Body weight changes (b) and survival rates (c) of mice following *S.*
793 *Typhimurium* SL1344 infection (n = 10 per group).

794 (d) Bacterial loads (CFU) in the liver, spleen, cecal contents, and blood at 2 dpi (n
795 = 6 per group). The dashed line indicates the limit of detection (LOD).

796 Data are shown as the mean ± SD. Statistical significance for body weight changes
797 and bacterial loads was assessed using two-way ANOVA; survival curves were
798 analyzed using the log-rank (Mantel-Cox) test. * $p < 0.05$; ** $p < 0.01$; *** $p < 0.001$;
799 ns, not significant.

800

801 **Figure 6. SKL targets the QseC histidine kinase to suppress *Salmonella***
802 **virulence and pathogenicity.**

803 (a) Inhibition of *S. Typhimurium* SL1344 biofilm formation by SKL and (SKL)₄ at the
804 indicated concentrations (1/4×, 1/2×, 1× MIC). PBS served as the vehicle control, and
805 polymyxin B at 4×MIC was used as a positive control.

806 (b) Quantitative real-time PCR (qRT-PCR) analysis of *qseC*, *phoP*, *lrp*, and *cpxA*
807 mRNA levels in *S. Typhimurium* SL1344 treated with PBS vehicle or SKL or (SKL)₄.

808 (c) qRT-PCR analysis of *qseC* mRNA levels in *S. Typhimurium* SL1344 following

809 treatment with vehicle or increasing concentrations of SKL ($\frac{1}{4}\times$, $\frac{1}{2}\times$, and $1\times$ MIC).

810 (d) Western blot analysis of QseC and RpoB (loading control) protein levels in wild-
811 type (WT), $\Delta qseC$ (*qseC* knockout), and complemented (C- $\Delta qseC$) *S. Typhimurium*
812 strains, with (+) or without (-) SKL treatment (upper panel). Densitometric quantification
813 of QseC protein levels relative to RpoB, normalized to the WT vehicle group (lower
814 panel).

815 (e) Schematic of the QseB/QseC two-component system regulon in *S. Typhimurium*
816 1344, depicting the regulation of *Salmonella* pathogenicity island 1 (SPI-1) genes (*hilD*,
817 *sipA*) for epithelial invasion, SPI-2 genes (*ssaV*, *sifA*) for intracellular replication, and
818 flagellar genes (*flhDC*, *fliC*) for motility and colonization.

819 (f-k) qRT-PCR analysis of *hilD* (f), *sipA* (g), *ssaV* (h), *sifA* (i), *flhDC* (j), and *fliC* (k)
820 mRNA levels in WT, $\Delta qseC$, and C- $\Delta qseC$ *S. Typhimurium* strains treated with PBS
821 vehicle or SKL at a subinhibitory concentration ($\frac{1}{4}\times$ MIC).

822 (l) Experimental scheme for competitive infection assay in mice.

823 (m) Competitive index in the indicated tissues from vehicle- and SKL-treated mice
824 (n = 6 per group).

825 Data are shown as the mean \pm SD. Statistical significance was assessed by two-
826 way ANOVA. * $p < 0.05$; ** $p < 0.01$; *** $p < 0.001$; ns, not significant.

827

828 **Figure 7. SKL and (SKL)₄ ointment exhibit potent therapeutic efficacy in a mouse**
829 **model of methicillin-resistant *Staphylococcus aureus* (MRSA) wound infection.**

830 (a) Schematic of experimental timeline of MRSA wound infection in mice.

831 (b) Representative photographs of wounds in MRSA-infected mice on 3, 5, 7, 9,
832 and 11 dpi following the indicated treatment.

833 (c) Wound closure kinetics in MRSA-infected mice over the treatment course.

834 (d) Percentage of wound healing at each indicated time point (n = 6 per group).

835 (e) Residual MRSA burden (CFU) in wound tissues after various treatments (n = 6
836 per group). The dashed line indicates the limit of detection (LOD).

837 Data are shown as the mean \pm SD. Statistical significance was determined by one-
838 way ANOVA or two-way ANOVA. * $p < 0.05$; ** $p < 0.01$; *** $p < 0.001$; ns, not significant.

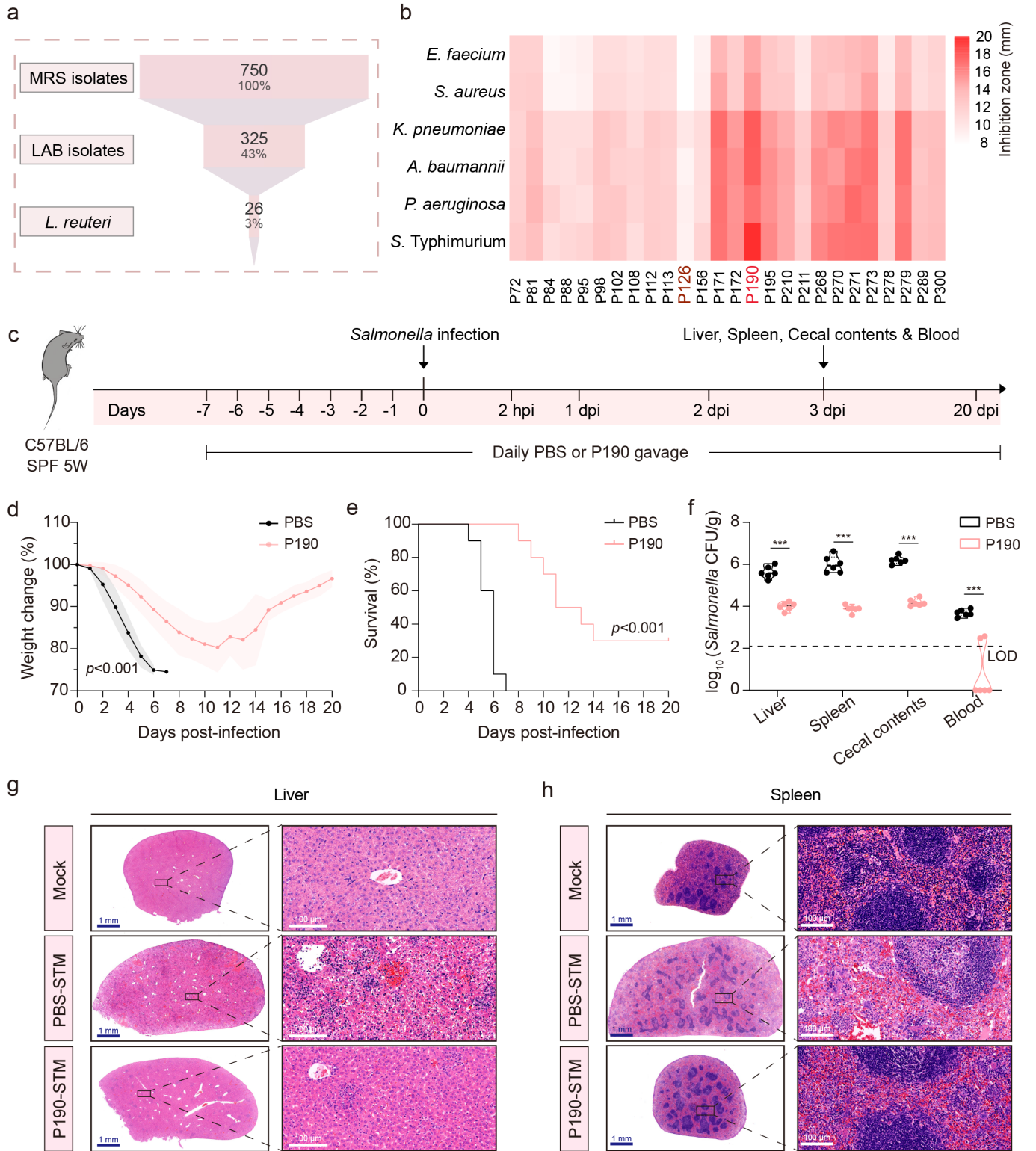
Fig 1

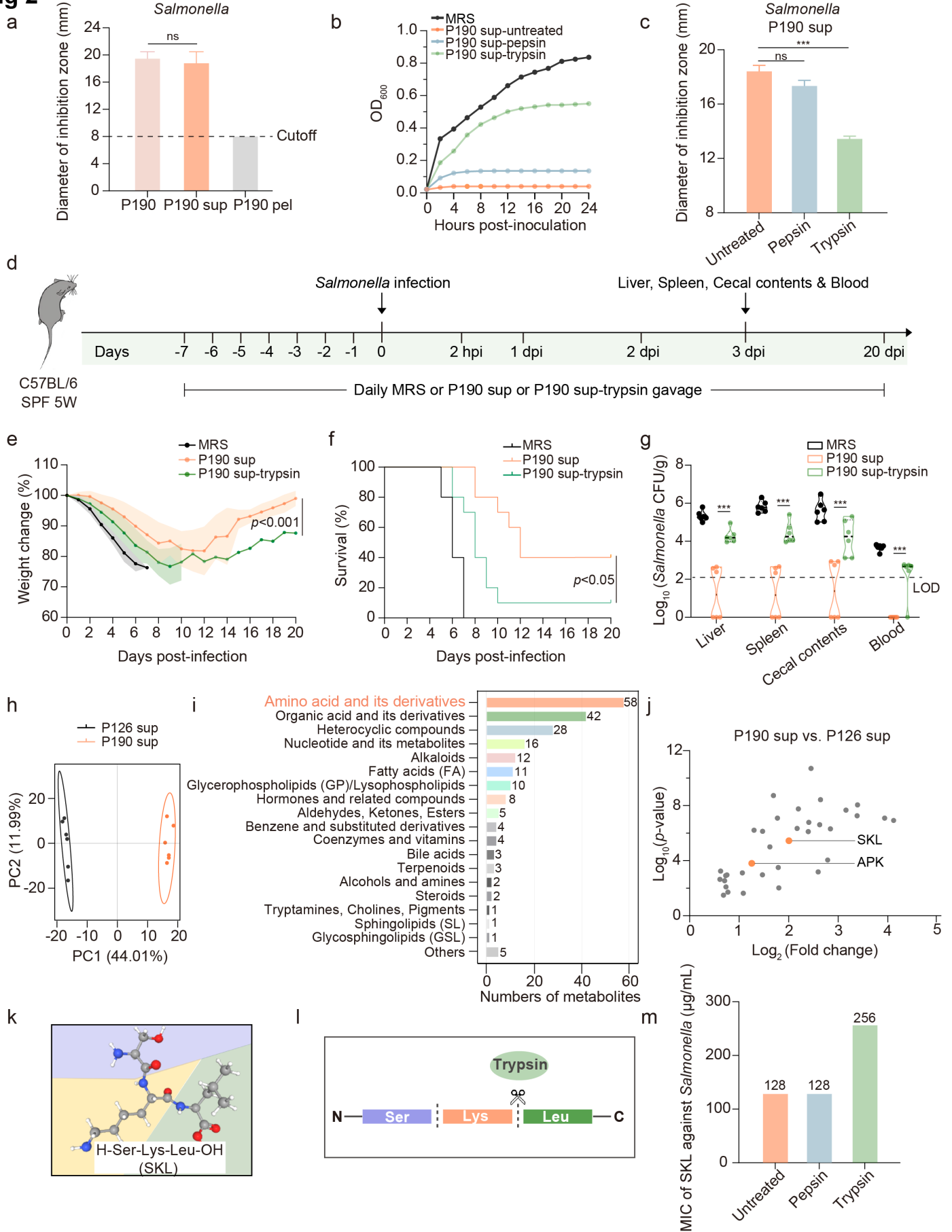
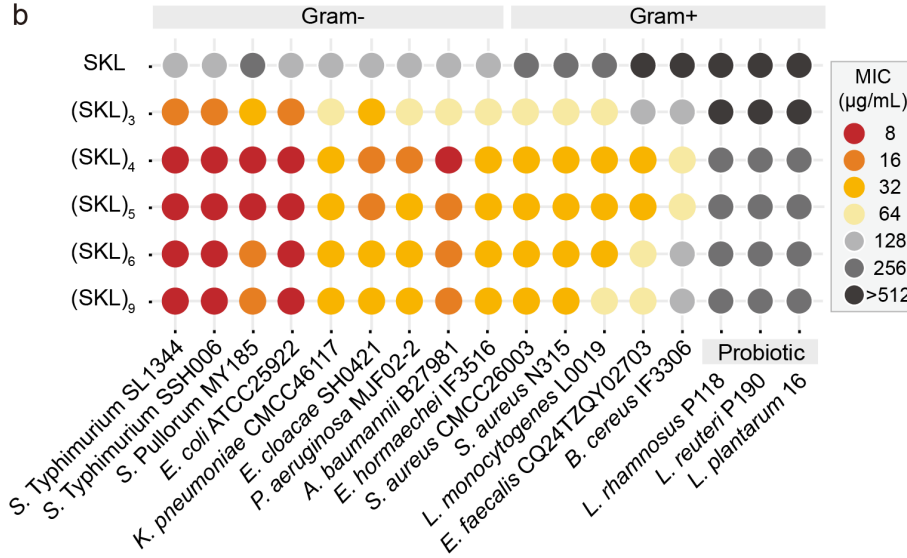
Fig 2

Fig 3

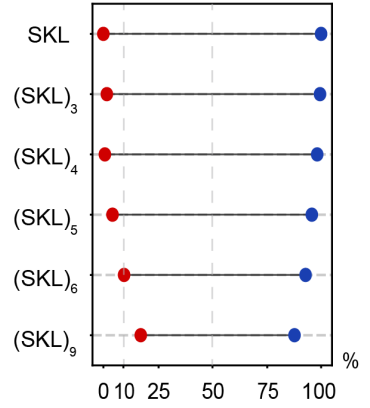
a



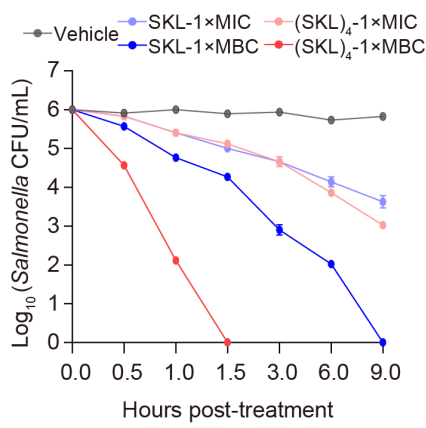
b



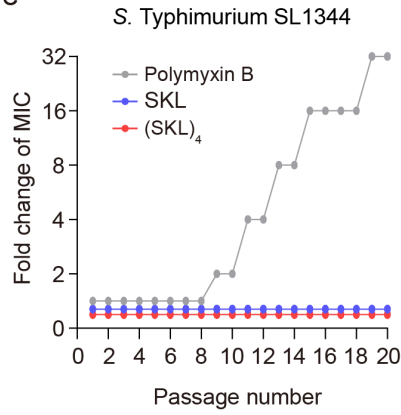
c



d



e



f

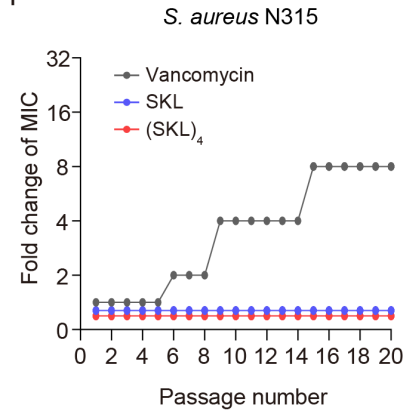


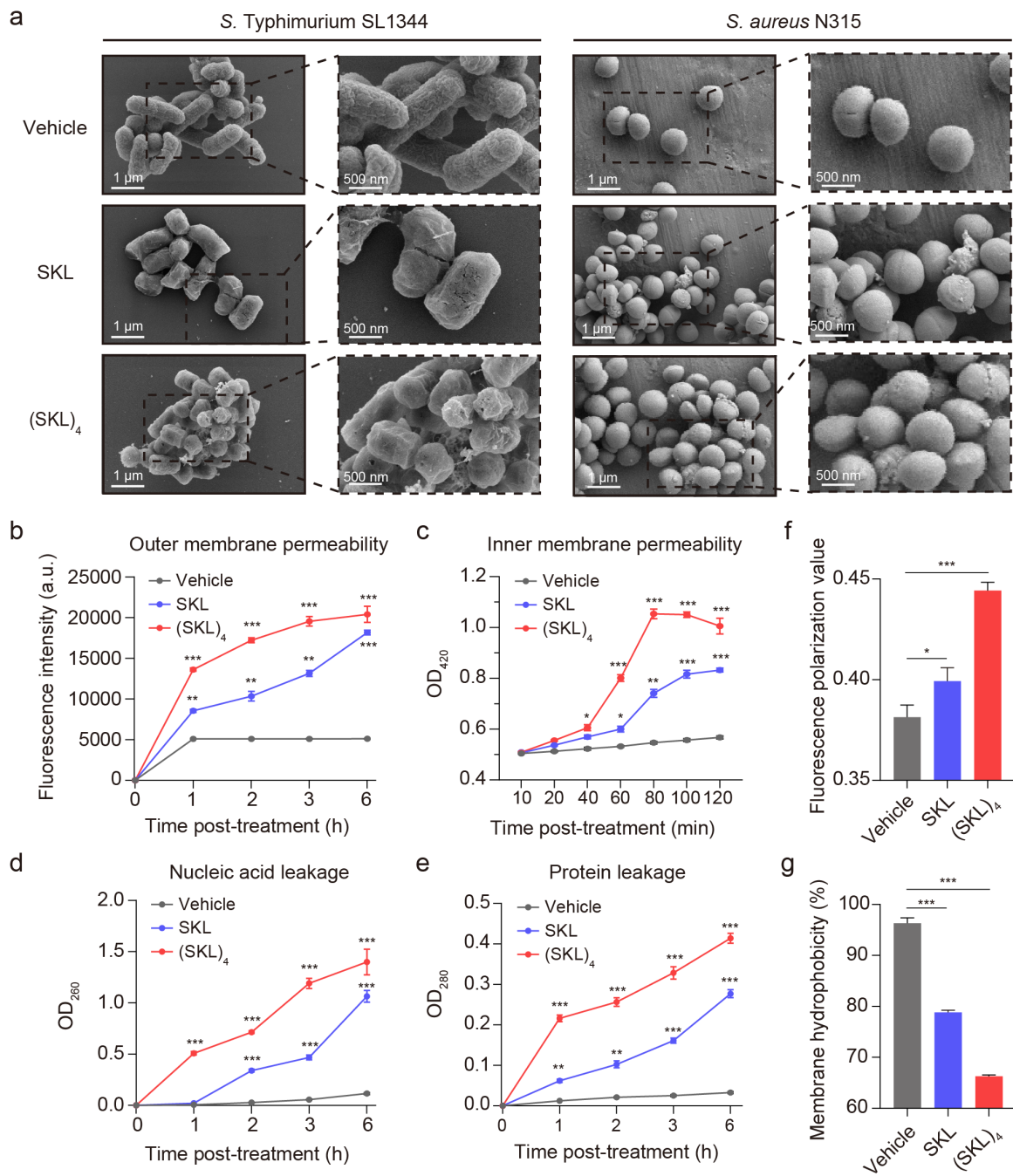
Fig 4

Fig 5

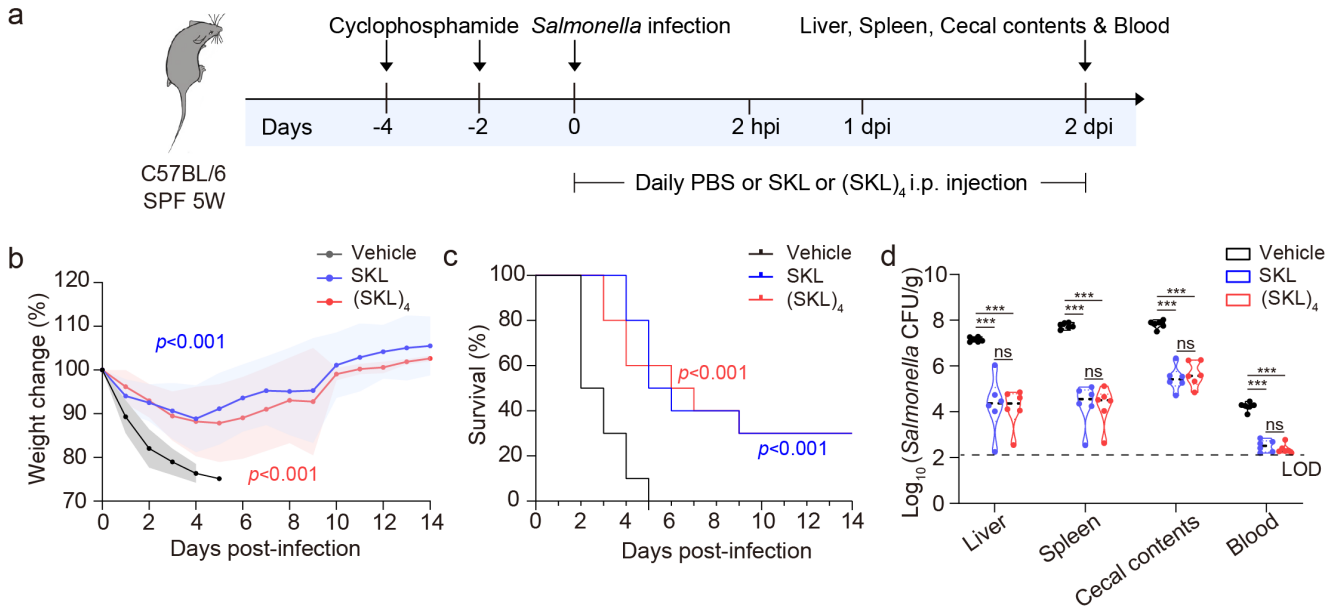


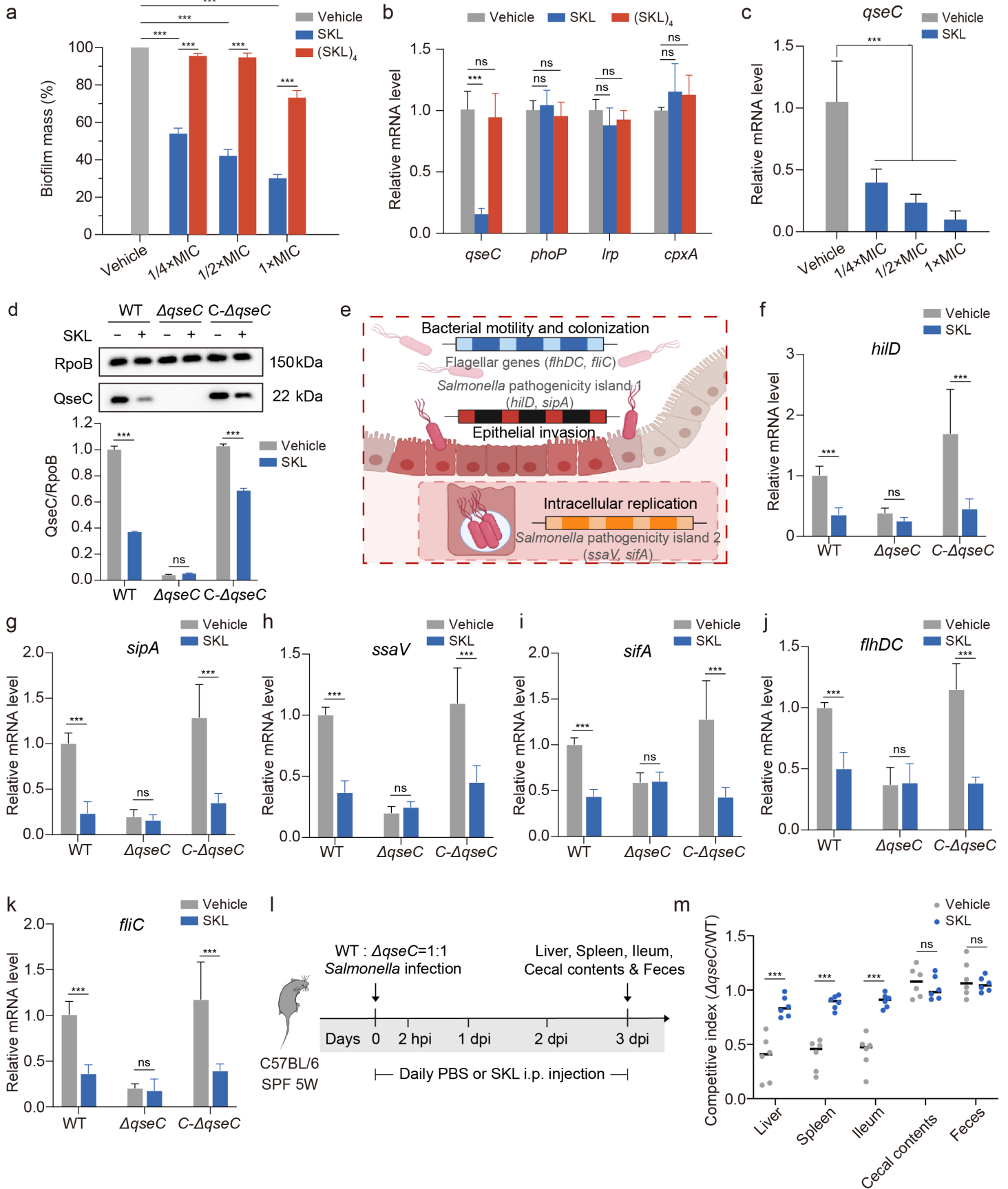
Fig 6

Fig 7

